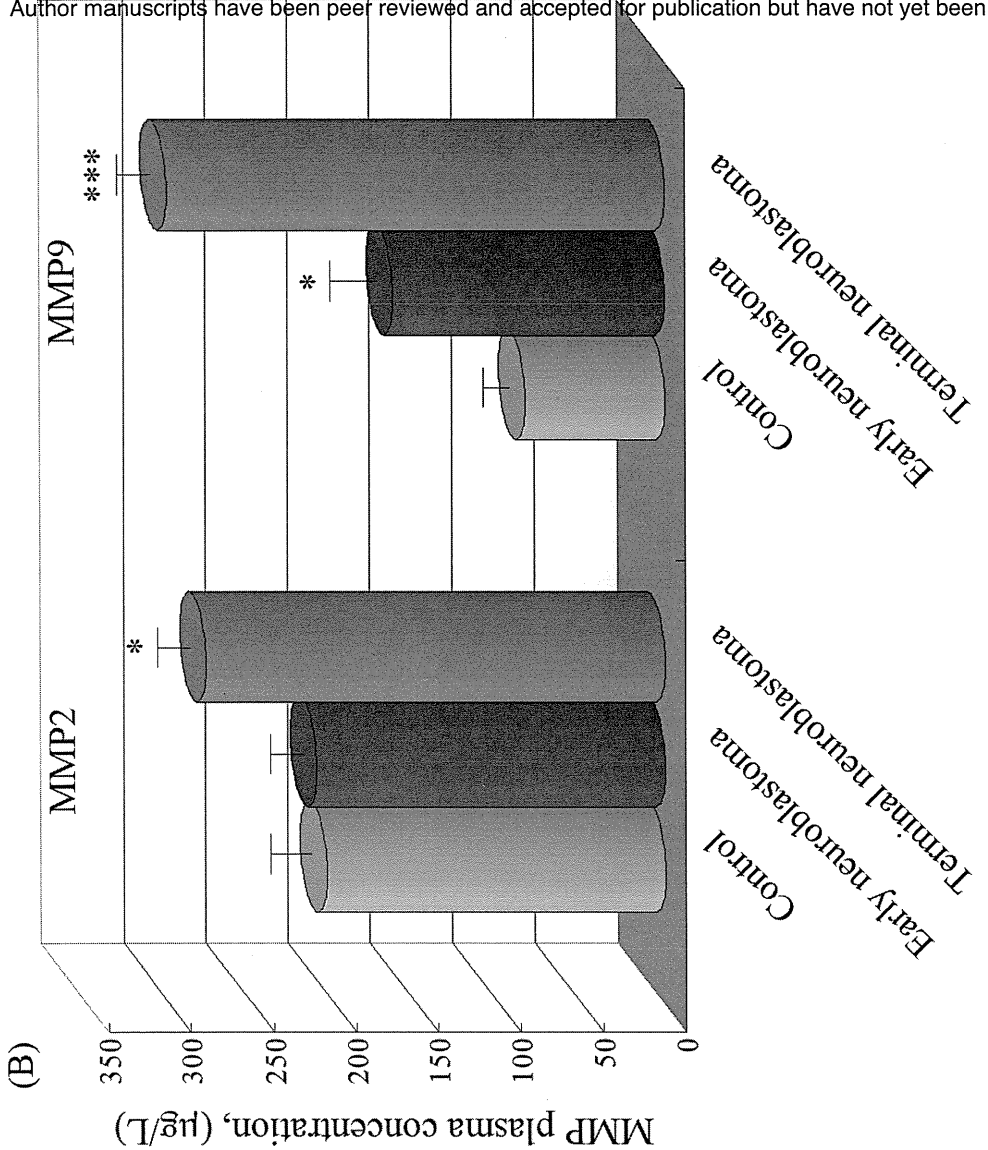

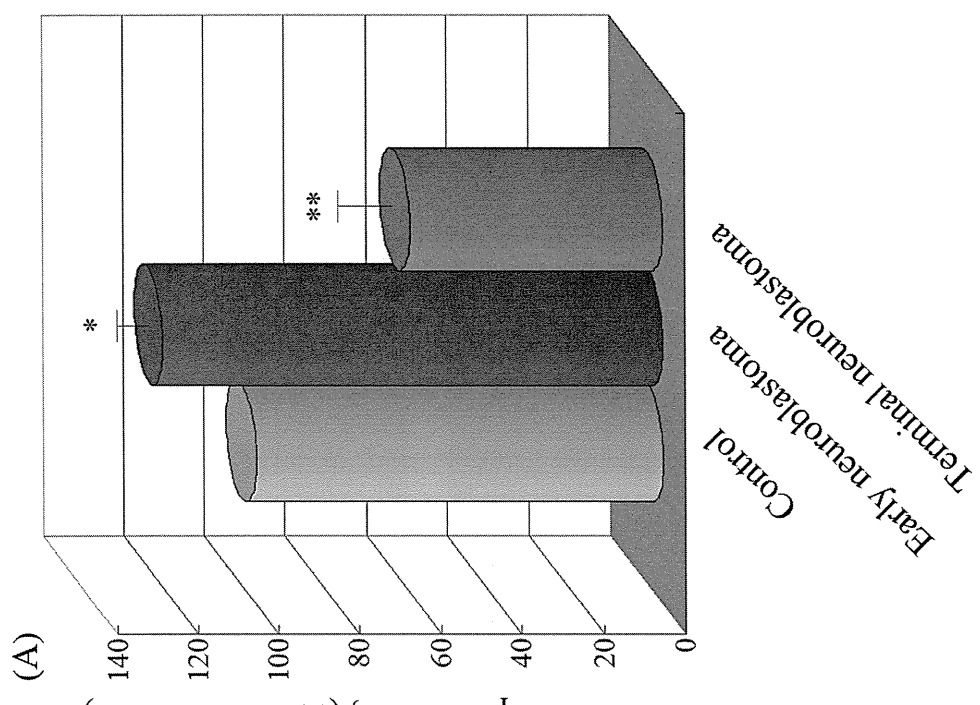

Figure 7

Figure 3

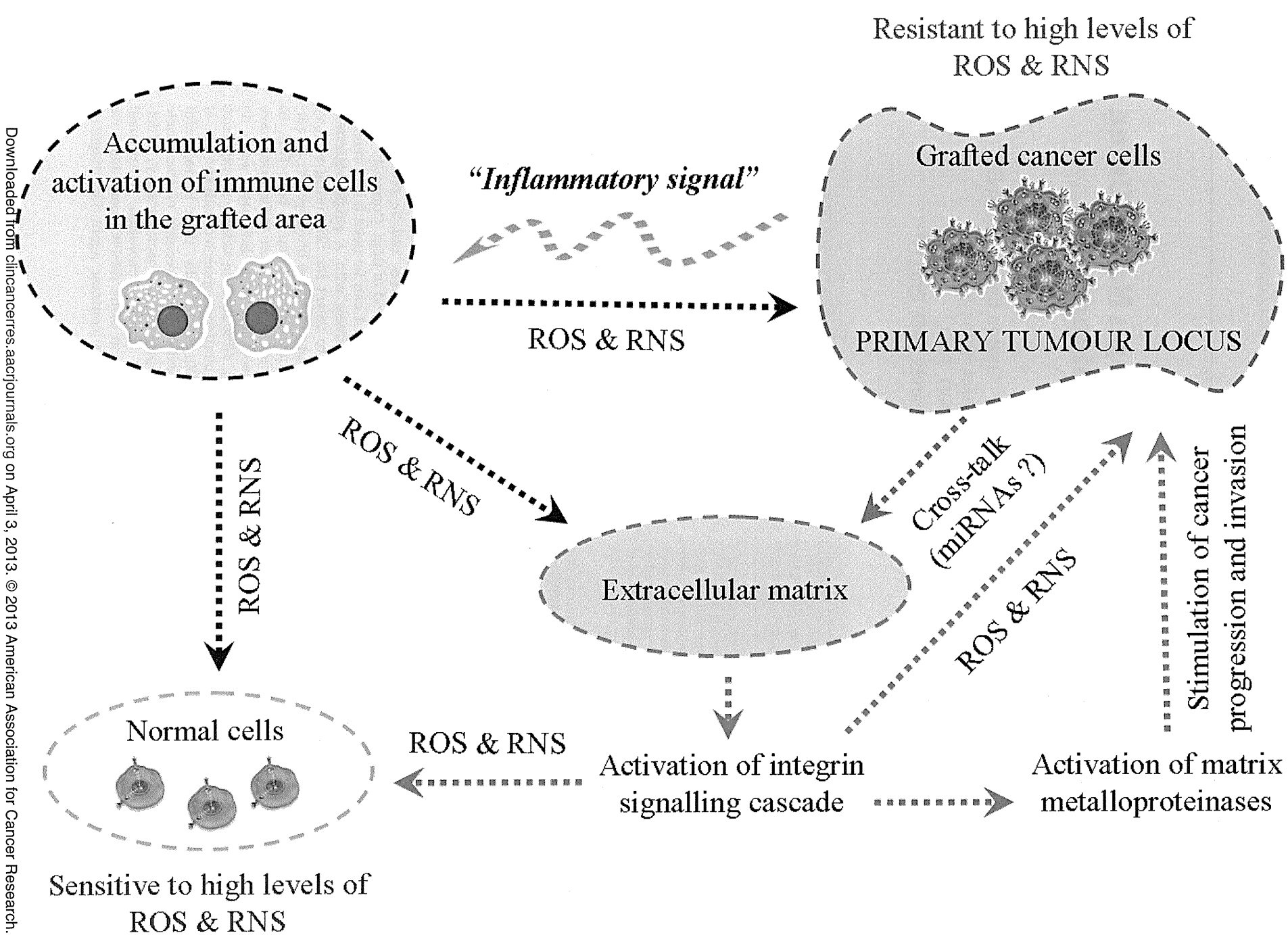

Figure 9

Original Research

In Vivo Identification of Sentinel Lymph Nodes Using MRI and Size-Controlled and Monodispersed Magnetite Nanoparticles

Shuji Iida, MD,[1] Kensuke Imai, MS,[2] Sachiko Matsuda, PhD,[1] Osamu Itano, MD, PhD,[1*] Mamoru Hatakeyama, PhD,[3] Satoshi Sakamoto, PhD,[2] Daisuke Kokuryo, PhD,[4] Koji Okabayashi, MD,[1] Takashi Endo, MD,[1] Yoshiyuki Ishii, MD, PhD,[1] Hirotoshi Hasegawa, MD, PhD,[1] Ichio Aoki, PhD,[4] Hiroshi Handa, MD, PhD,[2,3] and Yuko Kitagawa, MD, PhD[1]

Purpose: To develop a sentinel lymph node (SN) identification method using accurately synthesized magnetic nanoparticles (MNPs), as an enhanced specific SN tracer in combination with magnetic resonance imaging (MRI) in intact rodent and SN metastasis models.

Materials and Methods: Three sizes of MNPs were originally synthesized. We developed an experimental rat SN model, with brachial lymph nodes (Br) as the SN and the axillary lymph node (Ax) as the second lymph node, and injection of MNPs via the front paw. SN detectability was evaluated in vivo using T_1-weighted MR images after injection of the synthesized MNPs, and the amount of iron in the Br and in the Ax was assessed using inductively coupled plasma optical emission spectrometry.

Results: The highest ratios of the amount of iron in the Br versus the Ax were 3.1 and 3.3, using 20-nm MNPs after 2- and 24-hour injections. The appropriate dose and particle diameter for MRI detection was optimized, and the SN was optimally distinguished in the normal and metastatic rat models using MRI after a 0.4 mg/kg 20-nm MNP injection.

Conclusion: We developed and optimized a useful SN identification method using MRI in rodent models.

Key Words: magnetic nanoparticles; MRI; sentinel lymph node; detection
J. Magn. Reson. Imaging 2013; 000:000–000.

THE DETERMINATION OF THE SPREAD of metastatic cancer to lymph nodes (LNs) and the histopathological status of tumor draining regional LNs are significant predictors of recurrence and overall survival for most solid malignancies, and are often used to justify the stratification of patients for adjuvant therapy (1,2). The first LN that receives lymphatic drainage from a primary tumor is defined as a sentinel lymph node (SN), and when metastasis is not found in an SN, it almost certainly will not be present in more distal LNs. The primary benefit of SN mapping and biopsy is that it enables surgeons to avoid nontherapeutic LN dissection and the complications that can be caused. SN biopsy is currently used in various organs, such as the colon (3–5), esophagus (6,7), and gastrointestinal tract (6,8).

The ideal SN imaging agent needs to travel quickly through the lymphatic channels and be retained in the SN for a significant period of time. Currently there are no imaging agents that can be used both preoperatively and intraoperatively with a single injection. The techniques used to detect the SN during surgery have focused on the use of a vital blue dye (9), a radioactive tracer (10), or a combination of both (11). In the clinic, dye and radioactive tracer techniques have some problems associated with their use, such as anaphylactic shock, difficulties in detection, exposure to radiation, and limitations connected with the use of radioisotopes (12,13). Additionally, there is no useful method for preoperative SN screening of the whole body, with the exception of radioscintigraphy, which has relatively poor spatial resolution. Ultrasmall superparamagnetic iron oxide (USPIO) particles have been introduced as a contrast agent for magnetic

[1]Department of Surgery, School of Medicine, Keio University, Tokyo, Japan.
[2]Department of Biological Information, Graduate School of Bioscience and Biotechnology, Tokyo Institute of Technology, Yokohama, Japan.
[3]Solutions Research Laboratory, Tokyo Institute of Technology, Yokohama, Japan.
[4]Molecular Imaging Center, National Institute of Radiological Sciences (NIRS), Japan.

Contract grant sponsor: Special Coordination Funds for Promoting Science and Technology from the Japan Science and Technology Agency; Contract grant sponsor: Kakenhi (JSPS); Contract grant sponsor: Funding Program for World-Leading Innovative R&D on Science and Technology (FIRST Program).

*Address reprint requests to: O.I., Department of Surgery, School of Medicine, Keio University, 35 Shinanomachi, Shinjuku-ku, Tokyo 160-8582, Japan. E-mail: laplivertiger@gmail.com

Received September 9, 2012; Accepted February 11, 2013.
DOI 10.1002/jmri.24108
View this article online at wileyonlinelibrary.com.

resonance imaging (MRI) (14–16). Studies of patients with head and neck, urologic, pelvic, gastric, esophageal, and breast cancers have confirmed the improved detection of LN metastases with USPIO-enhanced MRI (14,17–22), but it remains difficult to identify the SN. USPIO particles are not suitable for SN identification because they can track beyond the first node and into the second echelon nodes.

SN localization of tracer is influenced by several factors that include method and site of injection, dose, and particle size. Of these, particle size is one of the most important, but there is no agreement concerning the optimal particle size of the ideal colloid.

To overcome these problems, new magnetic nanoparticles (MNPs) were developed as a specific tracer for SNs (23). To improve the specificity of SN targeting, our MNPs had two special features: size and stable dispersion in solution owing to the manufactured surface coating. The purpose of the present study was to evaluate if the improved MNPs can work as an SN-specific tracer and have sufficient detectability for SN identification using MRI.

MATERIALS AND METHODS

Animal Preparation

All animal protocols were approved by the animal research committees. Male Donryu rats (Sankyo Labo Service, Tokyo, Japan) aged 5 weeks and weighing 230 ± 8 g were used for the optimization of MNP size ($n = 8$) and the amount injected ($n = 8$). For SN detection by MRI, 5-week-old male Donryu rats (Japan SLC, Shizuoka, Japan) weighing 198.0 ± 2.5 g were used ($n = 9$). Two male F344/NJcl-rnu/rnu nude rats (CLEA Japan, Tokyo, Japan) aged 4 weeks and weighing 193 ± 16 g were used for the establishment of the metastatic model, and seven of these rats weighing 172.0 ± 6.9 g were used for SN detection by MRI. For toxicity evaluation, two 6-week-old female BALB/c mice (Oriental Yeast, Tokyo, Japan) were used for the high-dose group and four for the low-dose group. Animals were maintained on a standard laboratory chow diet and had access to tap water ad libitum. During the entire procedures, anesthesia was induced and maintained in rats by means of 4% isoflurane inhalational (Mylan, Tokyo, Japan), and they were then ventilated with 1.5% isoflurane and a 1:2 O_2/room air gas mixture using a mechanical carburetor. Ferucarbotran as a control was injected into the forepaws at the same iron concentration as that of the MNPs.

Cell Lines

Human epithelial carcinoma cell line A431 (American Tissue Culture Collection, Rockville, MD [ATCC]) was used for stable transfection with green fluorescent protein (GFP). A431 cells were maintained in Dulbecco's modified Eagle's medium (DMEM) with 10% heat-inactivated fetal bovine serum (Gibco, Grand Island, NY) in a 5% (v/v) CO_2 humidified incubator at 37°C.

Rat Sentinel Metastatic Model

To establish the metastatic model, 2×10^6 A431 cells that stably expressed GFP (1×10^7 cells/mL in phosphate-buffered saline [PBS]) were injected into the forepaw of 4-week-old male nude rats. LNs were extracted after 18 days of implantation, and metastasis was visualized under a fluorescence stereoscopic microscope.

Magnetite Nanoparticle Preparation

Three MNPs whose particle sizes were 4, 8, and 20 nm (abbreviated M4, M8, and M20, respectively) were prepared according to previous reports (23–25). Since the three MNPs were citrate-coated magnetite nanoparticles based on reported highly size-controlled nanocrystals (21), they are monodispersed in water. A conventional contrast agent, Ferucarbotran (Resovist, Fujifilm Pharma, Tokyo, Japan), was used as a control. Ferucarbotran is an MRI contrast agent that is a hydrophilic colloid composed of carboxydextran-coated iron oxide nanoparticles comprising multiple crystals. The overall hydrodynamic diameter of Ferucarbotran was 62.3 ± 18.7 nm measured using dynamic light scattering (FPAR-1000, Otsuka Electronics, Osaka, Japan).

Surgical and Histological Procedures

A skin incision was performed over the popliteal fossa after an enhancing agent was injected into the front paw using a microsyringe with a 27G needle, and these spaces were explored for lymphatic channels or LNs. At the completion of popliteal fossa exploration, samples of tissue were harvested from the brachial lymph nodes (Br) and the axillary lymph node (Ax) and were subsequently pathologically evaluated. Harvested LN tissues were fixed in 10% neutral buffered formaldehyde and were processed for paraffin embedding. Microsections (4 μm) were prepared with a microtome and were deparaffinized in xylol. They were then rehydrated in a descending ethanol series and stained with Prussian blue to detect iron particles in the cells.

Measurement of Magnetite in LNs

After injection of the agent, the Br and the Ax were harvested, weighed, and lyophilized. The lyophilized samples were dissolved in nitric acid. The amount of magnetite in the LNs was measured using inductively coupled plasma optical emission spectrometry (ICP-OES) (Perkin Elmer Optima 3000 XL ICP-OES Spectrometer, Kanagawa, Japan).

MRI

To examine whether or not the SN could be detected using MNPs in normal rats, and to determine if they could trace SNs with metastases in the metastatic rat model, they were injected into both forepaws. All MR images were acquired on a 7.0 T animal MRI (Magnet:

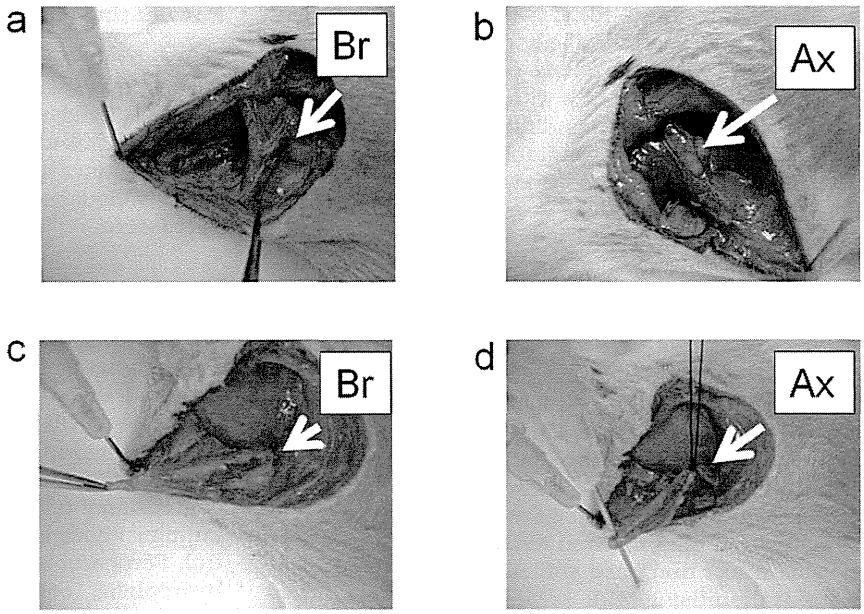

Figure 1. The brachial lymph node (Br) (**a**) and the axillary lymph node (Ax) (**b**) are shown. The lymphatic anatomy in the hind limb of the rat has been exposed to show the blue contiguously linked Br (**c**) and Ax (**d**) after injection of isosulfan blue into the front paw.

Kobelco, Kobe, Japan and JASTEC, Kobe, Japan; Console: Bruker Biospin, Ettlingen, Germany) with a 72-mm inner-diameter birdcage coil. Rats were initially anesthetized with 4.0% isoflurane (Mylan), orally intubated, and then ventilated with 1.5% isoflurane and a 1:2 O_2/room air gas mixture using a rodent ventilator (MRI-1: CWE, Ardmore, PA). Breaths per minute were set within a limit of 60–80. MRI scans were performed before and at 30 minutes after MNP injection. To avoid too strong a susceptibility effect in the MNPs, T_1-weighted contrast was employed using incoherent 2D gradient echo sequences (fast low-angle shot, FLASH) with fat suppression preparation pulse and respiratory gating. The parameters were as follows: TR/TE = 350–980/10 msec depending on respiratory gating; flip angle = 45°; slice thickness = 1.0 mm; slice gap = 0.5 mm; field of view = 60 × 60 mm^2; matrix = 256 × 256; number of slices = 13; and number of acquisitions = 4.

Exploratory MNP Single Toxicity Study

Mice were divided into five groups, and 20-nm MNPs were injected into the tail vein (control: saccharose fluid injection; low dose: 625 μmol/kg; medium-low dose: 1250 μmol/kg; medium-high dose: 2500 μmol/kg; and high dose: 5000 μmol/kg), which are the same doses as those tested in the toxicity study for Ferucarbotran according to the accompanying documentation from the manufacturer. Overall animal condition and weight changes were evaluated. Tissue samples of lung, liver, and spleen were examined histopathologically on postoperative day 7.

Data Analysis and Statistics

MR image analysis was performed using the MRVision image display and processing package (MRVision, Winchester, MA). Signal changes of LNs induced by MNPs were evaluated on MR images by two independent researchers. The negatively enhanced area (mm^2) in LNs was calculated by means of the ROI tool of the MRVision software. All results were expressed as the mean ± standard error. Statistical significance was determined using the Mann–Whitney *U*-test for MRI analysis. $P < 0.05$ was considered being statistically significant. In addition, all receiver operating characteristic (ROC) curve analyses of MRIs were carried out using the data from the negatively enhanced area. ROCs displaying sensitivity together with the false-positive rate (1-specificity) for detecting MNPs by MRI,

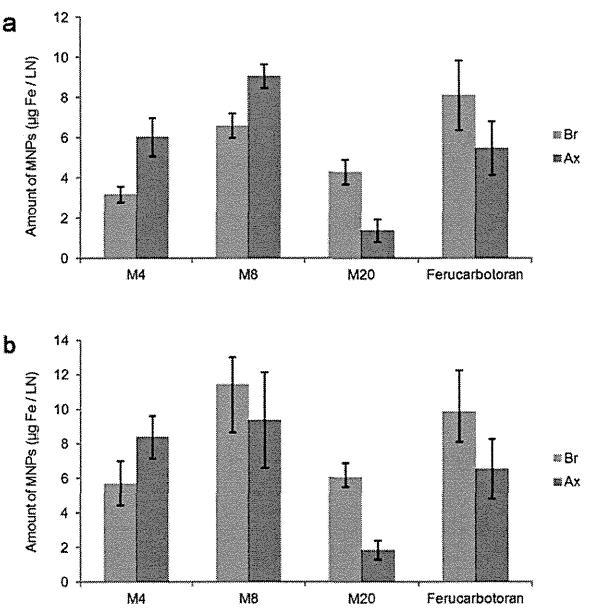

Figure 2. The amount of the three sizes of MNPs (M4, M8, and M20) and Ferucarbotran in the Br and Ax at 2 hours (**a**) and 24 hours (**b**) after injection.

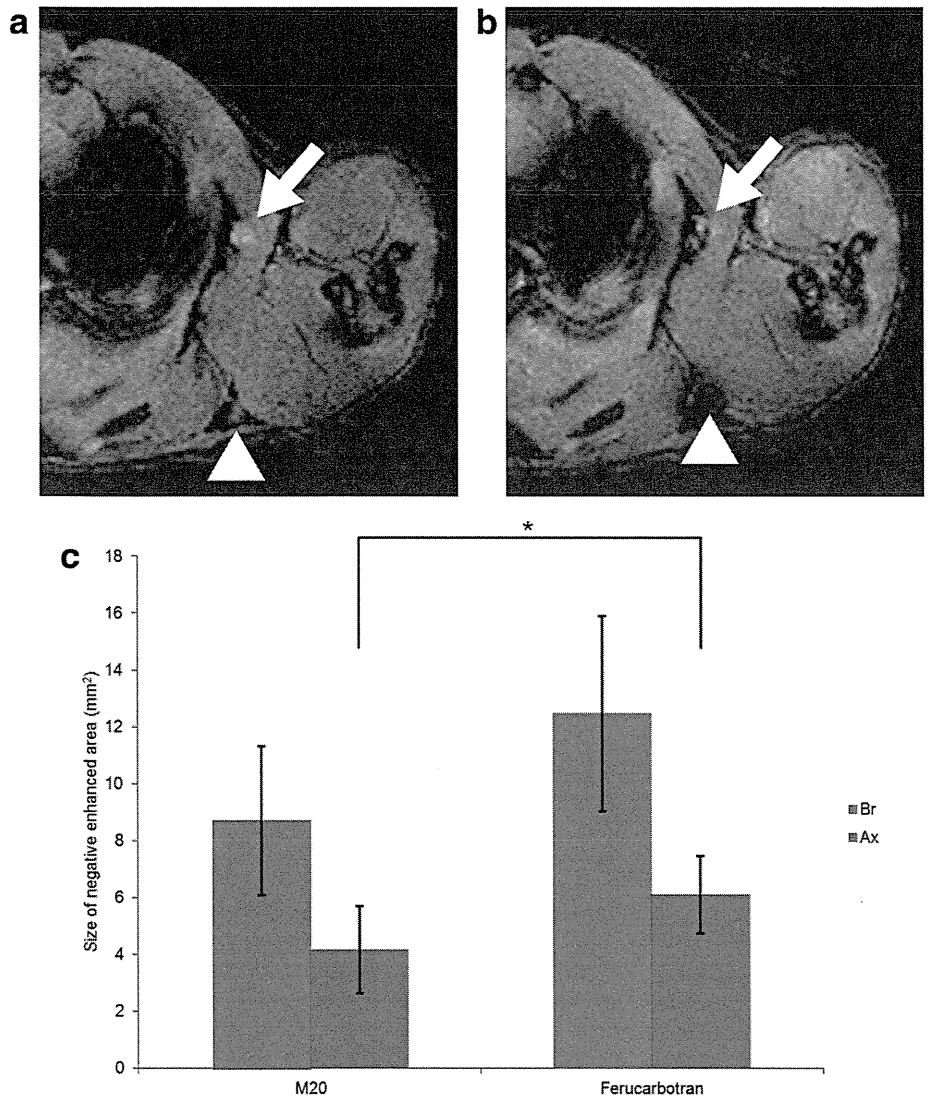

Figure 3. T_1-weighted gradient echo images obtained before (**a**) and after (**b**) magnetite administration in wildtype rats. The arrowhead indicates the Br and the arrow indicates the Ax. The sizes of the negative enhanced areas associated with M20-MNPs and Ferucarbotran nanoparticles are shown in (**c**).

and the area under the curve with 95% confidence intervals (CIs) were calculated. All statistical analyses were performed using Stat View v. 5.0 statistical software package (SAS Institute, Cary, NC).

RESULTS

Establishment of a Rat Model for SN Identification: Surgical Exposure

The Br in rats most often existed as three similarly sized (2–3 mm) nodes (Fig. 1a) and the Ax typically consisted of four to five nodes of 1–3 mm in size (Fig. 1b). To determine the SN of rats, the popliteal fossa was explored visually for any blue-colored lymphatic channels or LN within 3–5 minutes of injection of isosulfan blue into the front paw. The lymphatic anatomy in the hind limb of the rat was exposed to show blue contiguously linked Br (Fig. 1c) and Ax (Fig. 1d). The Br should represent the SN and the Ax should be a higher echelon node further downstream from the SN.

Determination of the Appropriate Diameter of MNPs as a Tracer for SN Identification

To investigate which was the most suitable diameter for a tracer, we measured and compared the levels of our MNPs (M4, M8, and M20) and Ferucarbotran in the Br and Ax at 2 hours (Fig. 2a) and 24 hours (Fig. 2b) after their injection by means of ICP-OES. For the initial experiment the dose of MNPs administered was 0.4 mg/kg according to the preliminary experiment. M20 was sustained in the SN and very little reached distant LNs even at 24 hours after injection. Conversely, M4, M8, and Ferucarbotran reached the Ax even after 2 hours. The ratio of the level of MNPs in the Br to the level of MNPs in the Ax was 3.1 after 2 hours and 3.3 after 24 hours using M20; this ratio

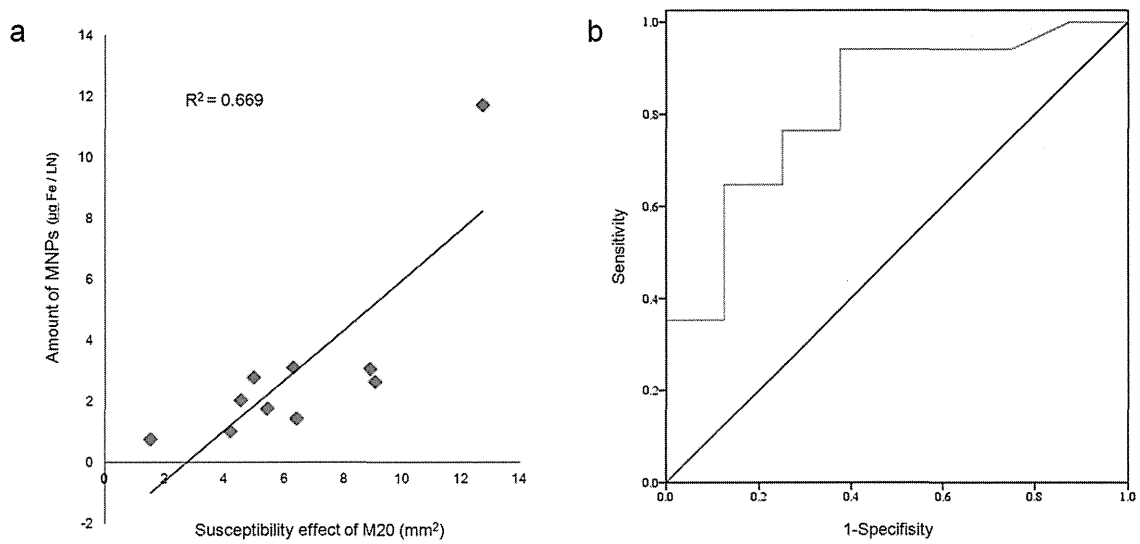

Figure 4. The optimal level of magnetite in the LN for MRI detection was evaluated. The relationship between the level of M20 in the LN and negatively enhanced area in the MR imaging is shown in direct proportion (R^2 = 0.669) (**a**). ROC curve analysis revealed that the threshold of the amount of magnetite required for MRI detection was 2.3 μg/LN (0.08 μg/mg tissue) with 76.5% sensitivity and 25% specificity, and the area under the ROC curve was 0.82 (95% CI, 0.64–1.0) (**b**).

was 0.5, 0.7, and 1.5 for M4, M8, and Ferucarbotran, respectively, after 2 hours, and 0.7, 1.2, and 1.5, respectively, after 24 hours. M20 had the highest ratio among these agents. This implied that M20 was the appropriate diameter for optimal identification of the SN in the SN models.

Determination of the Appropriate Amount of MNPs

Typical MR images are shown before (Fig. 3a) and after the injection of M20-MNPs (Fig. 3b). The influence of MNPs was evaluated in terms of the negatively enhanced area (mm^2) in MR images. In these images, clear signal reduction with a large susceptibility effect in the Br was observed after MNP injection, and there were no large alterations in the Ax. The average size of the negatively enhanced areas in the Ax measured using M20-MNPs (n = 5) was significantly smaller than those measured using Ferucarbotran (n = 4) (Fig. 3c). The results were mostly in agreement with the trend in the ICP-OEM results (Fig. 2). To determine the optimum level of magnetite in the LN for MRI detection, the relationship between the level of M20 in the LN and negatively enhanced area was evaluated. The relationship was in direct proportion as shown in Fig. 4a (R^2 = 0.669). In addition, analyses of the sensitivity and specificity of MRI detection were carried out. ROC curve analysis revealed that the threshold of the amount of magnetite required for MRI detection was 2.3 μg/LN (0.08 μg/mg tissue)

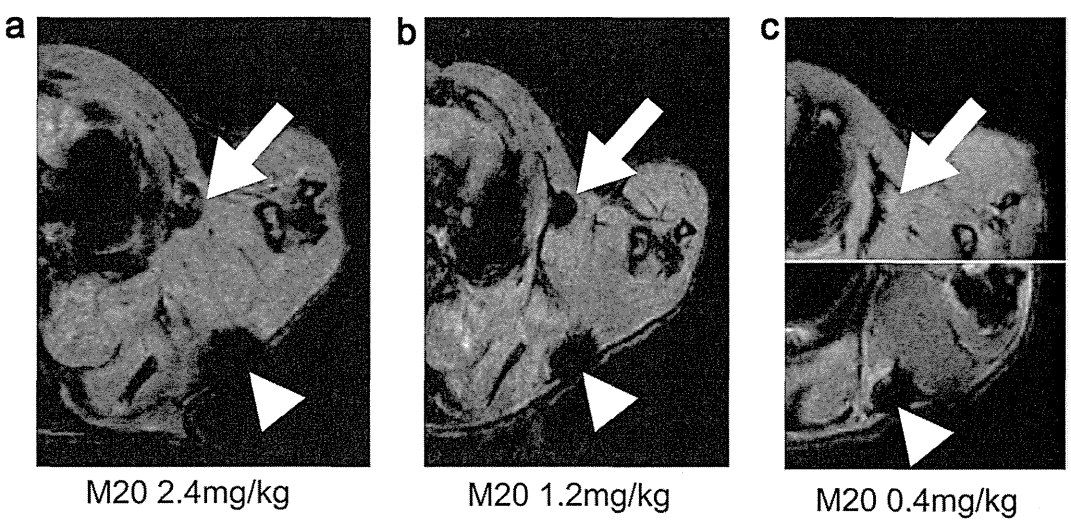

Figure 5. Comparison of the intensity level of the gradient echo image after 2.4 mg/kg (**a**), 1.2 mg/kg (**b**), and 0.4 mg/kg (**c**) injections of MNPs. The arrowhead indicates the Br and the arrow indicates the Ax.

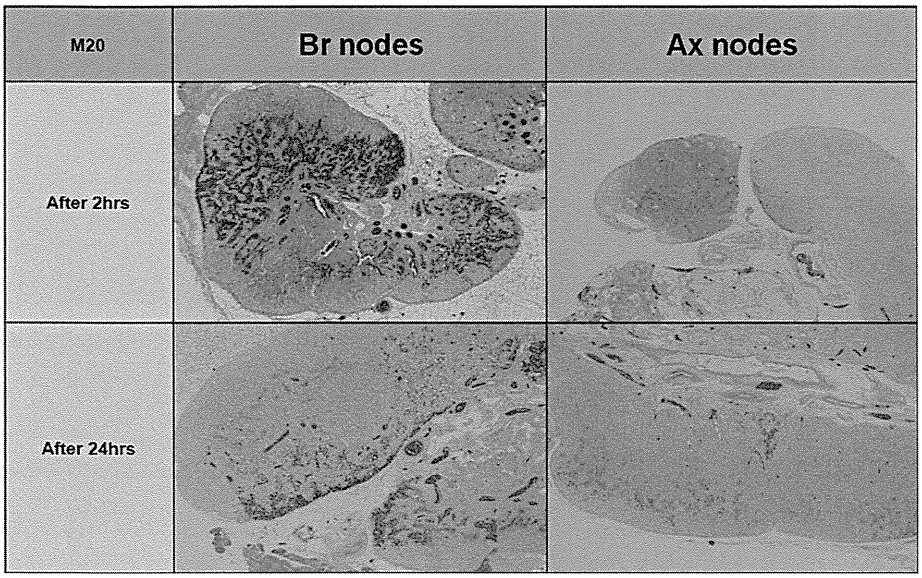

Figure 6. M20 MNPs in the Br and the Ax. The MNPs were injected into the rat front paw and the nodes were harvested after 2 and 24 hours. MNPs are colored blue owing to Prussian blue staining.

with 76.5% sensitivity and 25% specificity, and the area under the ROC curve was 0.82 (95% CI, 0.64–1.0) (Fig. 4b). The size of the signal reduction area evaluated may have been slightly larger than actual size because of the susceptibility effect, but detectability was improved.

Four different doses of M20 (2.4, 1.2, 0.4, and 0.2 mg/kg) were injected into the rat forepaw to find the optimal amount of MNPs for administration. In the case of M20 doses of 2.4 mg/kg and 1.2 mg/kg, signal intensity in both the Br and the Ax was decreased (Fig. 5a,b). The levels of MNPs in the Br and the Ax were 19.5 μg/Br (0.84 μg/mg tissue) and 3.2 μg/Ax (0.1 μg/mg tissue), respectively, in the case of the 2.4 mg/kg injection and 10.0 μg/Br (0.43 μg/mg) and 3.8 μg/Ax (0.12 μg/mg tissue), respectively, in the case of the 1.2 mg/kg injection. The level of MNPs in the Ax was higher than the threshold level 2.3 μg/LN (0.08 μg/mg tissue) for both the 2.4 mg/kg and 1.2 mg/kg injections, which indicated that not only the Br but also the Ax was detected by MRI. On the other hand, the signal intensity of the Br was decreased but that of the Ax did not change after a 0.4 mg/kg MNP injection (Fig. 5c). The level of MNPs in the Br was 0.94 μg/LN (0.04 μg/mg tissue) after a 0.2 mg/kg injection, and this was under the threshold. This implied that 0.4 mg/kg was the appropriate dose of injected magnetite to identify the SN in the case of M20 using rat SN models.

Pathological Evaluation

To confirm whether MNPs were retained in the Br after administration, the LN was evaluated pathologically using Prussian blue staining at 2 and 24 hours after injection of 0.4 mg/kg M20 (Fig. 6). MNPs were predominantly retained in the Br with very little in the Ax at both 2 and 24 hours. These results were consistent with the results described above. They confirmed that M20 was the MNP with appropriate diameter for SN identification and that 0.4 mg/kg was the optimal dose for injection.

Establishment of the Metastatic Rat Model and SN Identification Using MRI

At 18 days after the injection of A431 cells the Br and the Ax were harvested for evaluation. Fluorescent stereoscopic microscopy revealed metastatic tumor (Fig. 7a,b), and this was confirmed histologically with hematoxylin and eosin (H&E) staining (Fig. 7c) and a fluorescence microscope (Fig. 7d). Metastatic tumors were only seen in the Br and not in the Ax (data not shown). To evaluate if the SN was detectable in metastatic LNs, we performed an MRI experiment using the same procedure in the metastatic rat model at 18 days after A431 cell injection as that used in the normal rat model. Clear signal reduction in the Br with a large susceptibility effect was observed after MNP injection (Fig. 7e,f). In the metastatic and normal models, M20 accumulation in the Br was higher than in the Ax. This result indicated that 20-nm MNPs were selective and can be used as an SN tracer, even in the metastatic model.

Exploratory Single Toxicity Study of 20-nm MNPs

An exploratory single toxicity study was performed to evaluate the toxicity of the MNPs. Overall animal condition and body weight status were observed (Fig. 8). All of the mice (two out of two) in the high-dose group died within 1 minute after injection, and 50% of the mice (two out of four) died in the medium-high-dose group after 3 and 15 minutes. The other two mice in the medium-high-dose group exhibited weight loss on day 1. Both mice subsequently recovered from this initial weight loss. The tolerable dose of MNPs was the medium-low dose (1250 μmol/kg) injection. This indicated that the fatal dose was almost equal to that for Ferucarbotran. Histopathological analysis revealed

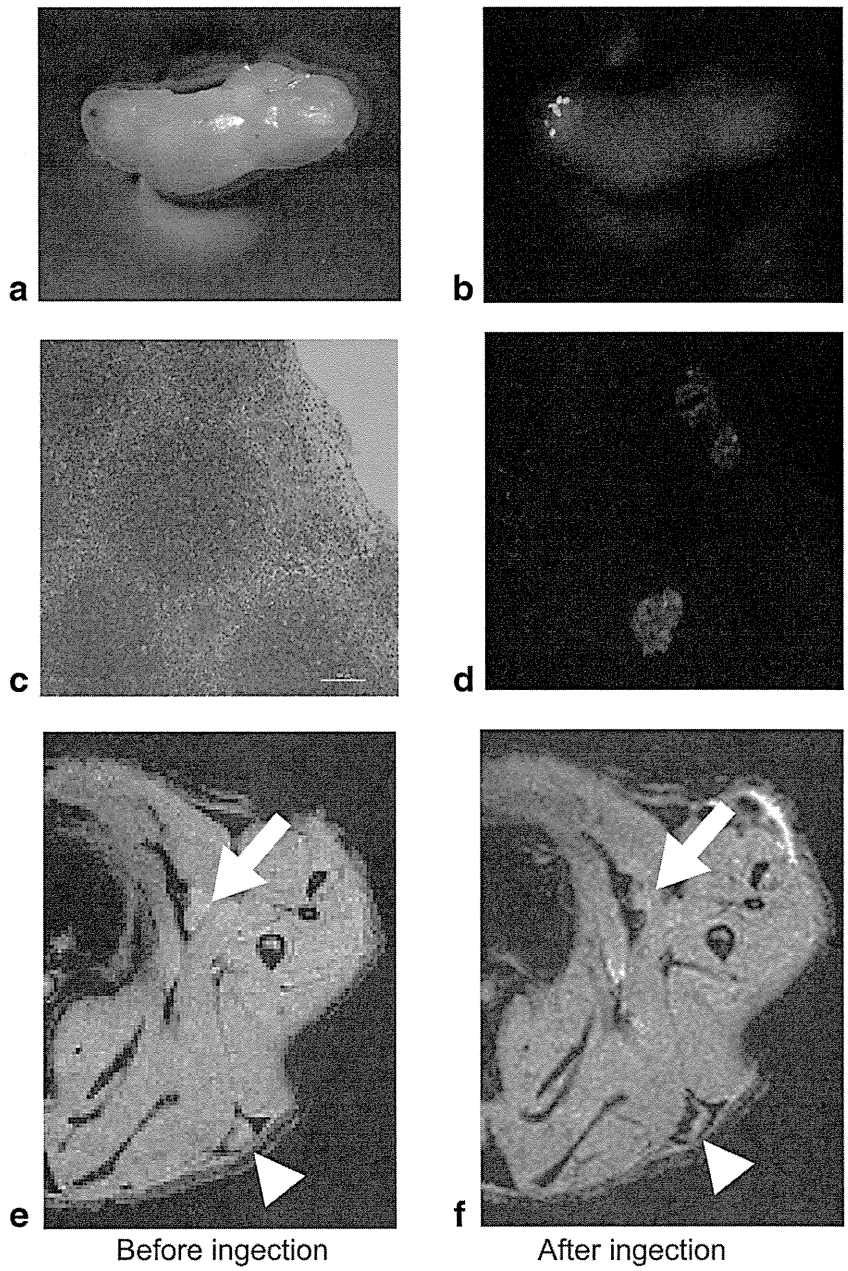

Figure 7. LN image at 18 days after A431 cell inoculation (**a**). A431 tumor transfected with green fluorescent protein (GFP) in the SN was visualized under a fluorescence stereoscopic microscope (**b**). The samples of tissue that were harvested from the Br were evaluated using H&E staining (**c**) and confirmed using a fluorescence microscope (**d**). Gradient echo images before injection (**e**) and after injection (**f**) show M20-MNPs in the tumor model. The arrowhead indicates the Br and the arrow indicates the Ax.

accumulation of MNPs in lung, liver, and spleen (Fig. 9a–r).

DISCUSSION

In the present study we demonstrated that our precisely sized 20-nm MNPs uniformly coated with citrate, used in combination with MRI, had good dispersion in solution and functioned as a specific SN detection agent, even in the case of metastatic nodes in the rodent model. The dye and radioactive tracer methods are the most widely used for identifying the SN from biopsies in cancer patients (26), but some disadvantages remain. The dye method can sometimes cause anaphylactic shock and has technical difficulties associated with SN detection. There are also technical difficulties associated with the use of the radioactive tracer method that include external γ-probe counting and radiation exposure. Radioscintigraphy is a whole-body screening technique that when used for preoperative SN screening has poor imaging spatial resolution, which limits its value for accurate identification of the detailed anatomy of the lymphatic drainage basin.

Our method using 20-nm MNPs has the potential to resolve these problems. MRI could be one of the useful methods for whole-body SN scanning, and has a number of potential advantages over radioscintigraphy. These include higher temporal resolution, higher

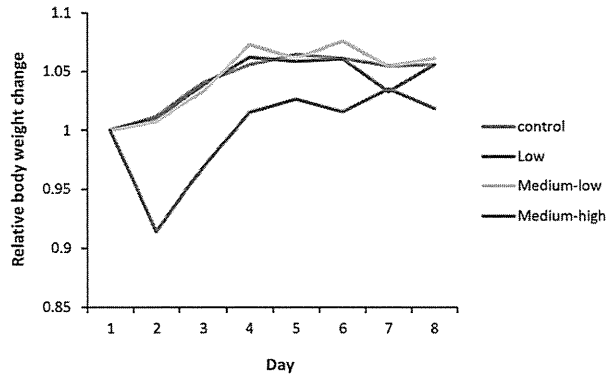

Figure 8. Weight change profile of animals after the administration of M20 MNPs into the tail vein. Control: saccharose fluid injection; Low dose: 625 μmol/kg; Medium-low dose: 1250 μmol/kg; Medium-high dose: 2500 μmol/kg; High dose: 5000 μmol/kg.

spatial resolution that enables the depiction of lymphatic channels, acquisition of 3Dimages, and the absence of radiation exposure. Generally speaking, MNPs can have potential ecytotoxic effects. One of the main mechanisms responsible for MNP cytotoxicity involves their response to reactive oxygen species (ROS); these are generated by the release of free iron ions and can lead to oxidative stress. ROS disturb the balance between oxidative pressure and antioxidant defense, which results in DNA damage (27,28). Previous studies have reported that USPIO-enhanced MRI is useful in the diagnosis of metastatic lymph nodes and that the use of this modality will be helpful in treatment decision-making for several organs (14,19–22). However, USPIO has been reported to have no specificity for the SN (29,30), and it remains difficult to identify the SN and to judge whether it has metastasis.

In contrast, our 20-nm MNPs demonstrated high selectivity for the SN, and their toxicity was the same as that of Ferucarbotran. MR lymphography with MNPs has the potential to enable us to predict the accurate anatomic location of the SN preoperatively in the clinic.

The special features of MNPs are uniform size, good dispersion in solution, and a surface coating (23). These features might influence their selective targeting of the SN. Particle size is one of the most important factors in SN identification (31). We explored the optimal size of MNPs by comparing 4-, 8-, and 20-nm MNPs with Ferucarbotran as a control, and found that 20-nm MNPs had the best diameter for SN identification. This diameter is within the range of several nm to a couple of hundred nm, as suggested by previous studies (31,32). Generally speaking, the effectiveness of the tracer draining into the lymphatic system depends on particle size. The smaller particles (diameters of less than 4–5 nm) are cleared from the injection site and exchanged through blood capillaries (33). The medium-sized particles (diameters of tens of nm) travel across the lymphatic capillaries and are trapped in the first LN (34). The larger particles (diameters of hundreds of nm) remain trapped at the injection site and can be retained for extended periods at the injection site (34). Bergqvist et al (35) found that both the total and specific uptake of particle colloids in parasternal LNs in rabbits was highest for when they had sizes between 10 and 50 nm.

Dose is another important factor in SN identification. In the present study we examined a range of doses of MNPs for SN identification using MRI. We found in the case of 20-nm MNPs, when evaluated in a rat model, that 0.4 mg/kg was the most appropriate amount. The level of 20-nm MNPs was found to be higher in the Br and lower in the Ax than the threshold value, only in the case of the 0.4 mg/kg injection dose. This was confirmed pathologically. In addition, in clinical use it is necessary to be able to detect the SN, even if micrometastasis is present. Lymphatic flow could change when metastasis exists in the LN. In our study, we established a metastatic rat model, and as was the case with our normal rat model, 20-nm MNP proved to be an ideal tracer for use with MRI.

There are other possible factors that could influence SN localization using MNPs; for example, the surface coating material and the surface electric charge. The benefit of our 20-nm MNPs is uniform size and good dispersion in solution. These are important factors in obtaining reproducible results. MNPs that are larger than 20 nm in size easily adhere to each other owing to magnetic attraction, and as a consequence good dispersion in solution is not possible (23). The surface charge on our MNPs and Ferucarbotran was approximately −40 mV. The surfaces of our MNPs are coated with citric acid, whereas the surfaces of the Ferucarbotran particles are coated with carboxydextran (23). Ferucarbotran that has an overall hydrodynamic diameter of 62 nm easily reached the distant node.

It has been reported that macrophages can influence the accumulation of SPIO in lymph nodes (18,36,37). The other characteristic feature of our MNPs is that they travel quickly (30 min) through lymphatic channels, and are retained in the SN for a significant period of time that exceeds 24 hours; however, the excretion time of the MNPs was not examined in our study.

Our 20-nm MNPs exhibited special characteristics that make them a useful SN tracer with the potential to solve the above-mentioned problems associated with the use of other tracer techniques. MRI with 20-nm MNPs as an SN tracer was confirmed as a high-resolution SN identification method that could potentially replace radioscintigraphy as a preoperative SN mapping method. In addition, our MNPs have potential as an SN tracer for intraoperative SN detection. The phenomenon known as magneto-acoustics, which involves sonic-wave emission by magnetically stimulated MNPs, was discovered in 1994 (38). We are in the process of developing a handheld device for SN detection during surgery. Using our 20-nm MNPs, we believe that in the near future we will be able to detect the SN before surgery using MRI and during surgery using our handheld device in the operating room.

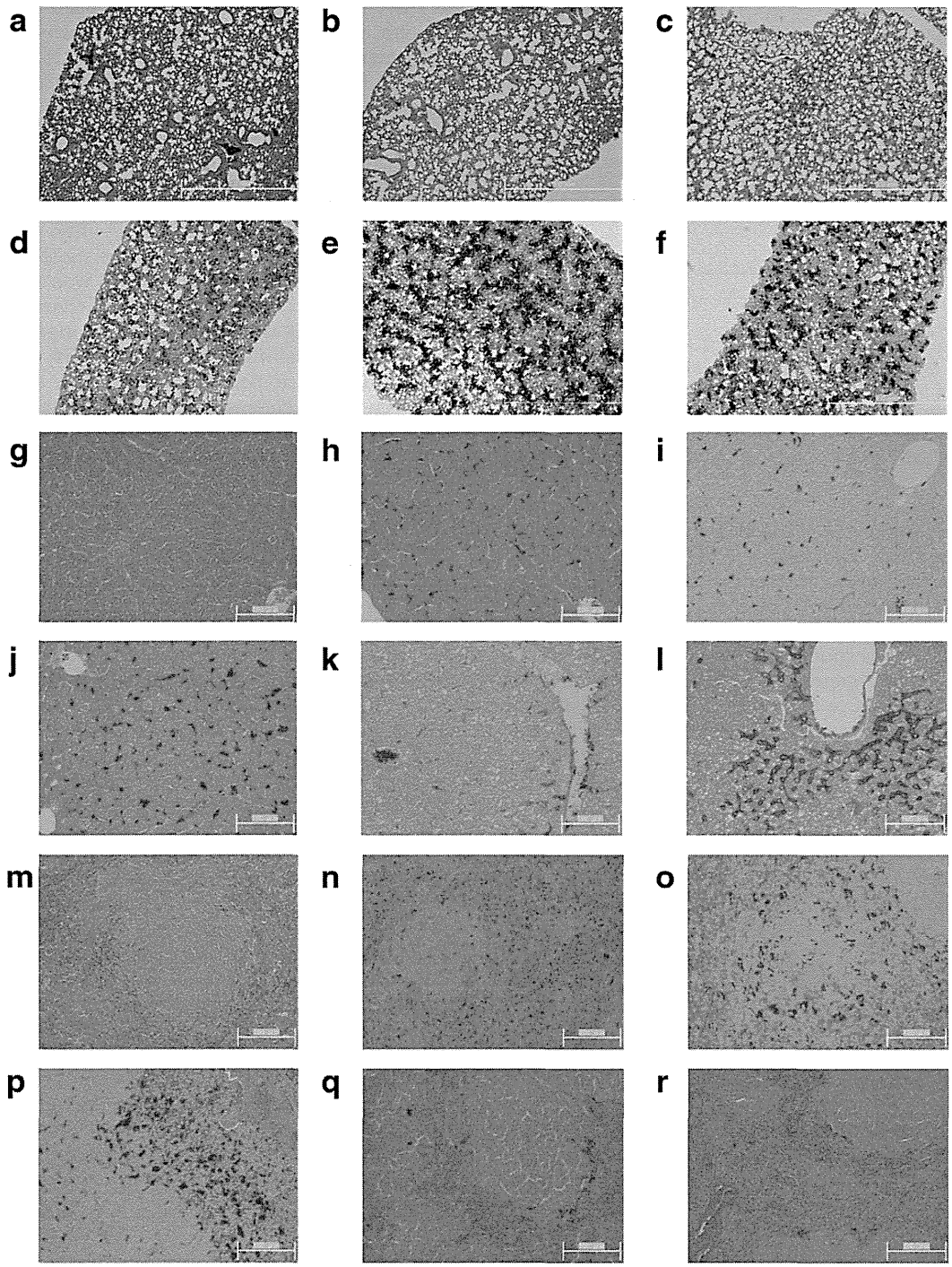

Figure 9. Prussian blue-stained tissue sections of lung/liver/spleen in the control group (**a/g/m**), in the low-dose group (**b/h/n**), in the medium-low dose group (**c/i/o**), in the medium-high-dose group (alive; **d/j/p**), in the medium-high-dose group (dead; **e/k/q**), and in the high-dose group (**f/l/r**).

In conclusion, we have developed a new MNP that is an ideal SN tracer and a useful SN identification method, using MRI with 20-nm MNPs as an SN tracer in rodent SN and SN metastasis models. This tracer could solve the problems associated with the use of other tracer techniques.

ACKNOWLEDGMENTS

The authors thank Masakazu Ueda, MD, PhD (Department of Surgery, School of Medicine, Keio University) for valuable discussion and continuing interest and encouragement, who died before the article

was completed. We thank Sayaka Shibata (NIRS) and Toshihide Muramatsu for assistance with experiments involving MRI measurements.

REFERENCES

1. Eifel P, Axelson JA, Costa J, et al. National Institutes of Health Consensus Development Conference Statement: adjuvant therapy for breast cancer, November 1-3, 2000. J Natl Cancer Inst 2001; 93:979–989.
2. Yoshino I, Nakanishi R, Osaki T, et al. Unfavorable prognosis of patients with stage II non-small cell lung cancer associated with macroscopic nodal metastases. Chest 1999;116:144–149.
3. Esser S, Reilly WT, Riley LB, Eyvazzadeh C, Arcona S. The role of sentinel lymph node mapping in staging of colon and rectal cancer. Dis Colon Rectum 2001;44:850–854; discussion 854–856.
4. Paramo JC, Summerall J, Wilson C, et al. Intraoperative sentinel lymph node mapping in patients with colon cancer. Am J Surg 2001;182:40–43.
5. Saha S, Bilchik A, Wiese D, et al. Ultrastaging of colorectal cancer by sentinel lymph node mapping technique—a multicenter trial. Ann Surg Oncol 2001;8(9 Suppl):94S–98S.
6. Kitagawa Y, Fujii H, Mukai M, et al. Intraoperative lymphatic mapping and sentinel lymph node sampling in esophageal and gastric cancer. Surg Oncol Clin N Am 2002;11:293–304.
7. Takeuchi H, Fujii H, Ando N, et al. Validation study of radioguided sentinel lymph node navigation in esophageal cancer. Ann Surg 2009;249:757–763.
8. Kitagawa Y, Kubota T, Otani Y, et al. [Clinical significance of sentinel node navigation surgery in the treatment of early gastric cancer.] Nippon Geka Gakkai Zasshi 2001;102:753–757.
9. Bergkvist L, Frisell J, Liljegren G, Celebioglu F, Damm S, Thorn M. Multicentre study of detection and false-negative rates in sentinel node biopsy for breast cancer. Br J Surg 2001;88:1644–1648.
10. Krag DN, Weaver DL, Alex JC, Fairbank JT. Surgical resection and radiolocalization of the sentinel lymph node in breast cancer using a gamma probe. Surg Oncol 1993;2:335–339; discussion 340.
11. Albertini JJ, Lyman GH, Cox C, et al. Lymphatic mapping and sentinel node biopsy in the patient with breast cancer. JAMA 1996;276:1818–1822.
12. Klausen TL, Chakera AH, Friis E, Rank F, Hesse B, Holm S. Radiation doses to staff involved in sentinel node operations for breast cancer. Clin Physiol Funct Imaging 2005;25:196–202.
13. Mertes PM, Malinovsky JM, Mouton-Faivre C, et al. Anaphylaxis to dyes during the perioperative period: reports of 14 clinical cases. J Allergy Clin Immunol 2008;122:348–352.
14. Anzai Y, Blackwell KE, Hirschowitz SL, et al. Initial clinical experience with dextran-coated superparamagnetic iron oxide for detection of lymph node metastases in patients with head and neck cancer. Radiology 1994;192:709–715.
15. Bellin MF, Roy C, Kinkel K, et al. Lymph node metastases: safety and effectiveness of MR imaging with ultrasmall superparamagnetic iron oxide particles—initial clinical experience. Radiology 1998;207:799–808.
16. Bulte JW, Kraitchman DL. Iron oxide MR contrast agents for molecular and cellular imaging. NMR Biomed 2004;17:484–499.
17. Kitamura N, Kosuda S, Araki K, et al. Comparison of animal studies between interstitial magnetic resonance lymphography and radiocolloid SPECT/CT lymphoscintigraphy in the head and neck region. Ann Nucl Med 2012;26:281–285.
18. Weissleder R, Elizondo G, Josephson L, et al. Experimental lymph node metastases: enhanced detection with MR lymphography. Radiology 1989;171:835–839.
19. Anzai Y, Prince MR. Iron oxide-enhanced MR lymphography: the evaluation of cervical lymph node metastases in head and neck cancer. J Magn Reson Imaging 1997;7:75–81.
20. Harisinghani MG, Saini S, Slater GJ, Schnall MD, Rifkin MD. MR imaging of pelvic lymph nodes in primary pelvic carcinoma with ultrasmall superparamagnetic iron oxide: preliminary observations. J Magn Reson Imaging 1997;7:161–163.
21. Nishimura H, Tanigawa N, Hiramatsu M, Tatsumi Y, Matsuki M, Narabayashi I. Preoperative esophageal cancer staging: magnetic resonance imaging of lymph node with ferumoxtran-10, an ultrasmall superparamagnetic iron oxide. J Am Coll Surg 2006;202: 604–611.
22. Tatsumi Y, Tanigawa N, Nishimura H, et al. Preoperative diagnosis of lymph node metastases in gastric cancer by magnetic resonance imaging with ferumoxtran-10. Gastric Cancer 2006;9: 120–128.
23. Hatakeyama M, Kishi H, Kita Y, et al. A two-step ligand exchange reaction generates highly water-dispersed magnetic nanoparticles for biomedical applications. J Mater Chem 2011; 21:5959–5966.
24. Park J, An K, Hwang Y, et al. Ultra-large-scale syntheses of monodisperse nanocrystals. Nat Mater 2004;3:891–895.
25. Sun S, Zeng H, Robinson DB, et al. Monodisperse MFe2O4 (M = Fe, Co, Mn) nanoparticles. J Am Chem Soc 2004;126:273–279.
26. Krag D. Minimal invasive staging for breast cancer: clinical experience with sentinel lymph node biopsy. Semin Oncol 2001;28: 229–235.
27. Ding J, Tao K, Li J, Song S, Sun K. Cell-specific cytotoxicity of dextran-stabilized magnetite nanoparticles. Colloids Surf B Biointerfaces 2010;79:184–190.
28. Lewinski N, Colvin V, Drezek R. Cytotoxicity of nanoparticles. Small 2008;4:26–49.
29. Rogers JM, Jung CW, Lewis J, Groman EV. Use of USPIO-induced magnetic susceptibility artifacts to identify sentinel lymph nodes and lymphatic drainage patterns. I. Dependence of artifact size with subcutaneous Combidex dose in rats. Magn Reson Imaging 1998;16:917–923.
30. Torchia MG, Nason R, Danzinger R, Lewis JM, Thliveris JA. Interstitial MR lymphangiography for the detection of sentinel lymph nodes. J Surg Oncol 2001;78:151–156; discussion 157.
31. Jimenez IR, Roca M, Vega E, et al. Particle sizes of colloids to be used in sentinel lymph node radiolocalization. Nucl Med Commun 2008;29:166–172.
32. Higashi H, Natsugoe S, Uenosono Y, et al. Particle size of tin and phytate colloid in sentinel node identification. J Surg Res 2004; 121:1–4.
33. Henze E, Schelbert HR, Collins JD, Najafi A, Barrio JR, Bennett LR. Lymphoscintigraphy with Tc-99m-labeled dextran. J Nucl Med 1982;23:923–929.
34. Keshtgar MR, Ell PJ. Sentinel lymph node detection and imaging. Eur J Nucl Med 1999;26:57–67.
35. Bergqvist L, Strand SE, Persson BR. Particle sizing and biokinetics of interstitial lymphoscintigraphic agents. Semin Nucl Med 1983;13:9–19.
36. Tanoura T, Bernas M, Darkazanli A, et al. MR lymphography with iron oxide compound AMI-227: studies in ferrets with filariasis. AJR Am J Roentgenol 1992;159:875–881.
37. Vassallo P, Matei C, Heston WD, McLachlan SJ, Koutcher JA, Castellino RA. Characterization of reactive versus tumor-bearing lymph nodes with interstitial magnetic resonance lymphography in an animal model. Invest Radiol 1995;30:706–711.
38. Roth BJ, Basser PJ, Wikswo JP Jr. A theoretical model for magneto-acoustic imaging of bioelectric currents. IEEE Trans Biomed Eng 1994;41:723–728.

通巻第755号 昭和42年2月6日第三種郵便物認可(毎月1回1日発行) 平成25年1月1日発行

ISSN 0451-2014

化学工業

CHEMICAL INDUSTRY

2013
VOL.64 NO.1
1

■特集／次世代健康・医療・福祉の科学

化学工業社

切らずに治すがん治療薬の開発

石川義弘[*1]・江口晴樹[*2]

1．はじめに

悪性新生物，いわゆる「がん」は，心疾患，脳血管疾患と並び，現在のわが国における3大死亡原因である．悪性新生物による死亡は，平成21年には34万4105人となっている[1]．この数字は前年度に比べて1000人以上の増加であり，人口の高齢化とともに，がんの国民疾患に占める重要性は，ますます増加すると考えられる．がんの種類でいうと，かつて首位を占めていた胃がんが減少傾向にあり，大腸がんや肺がんにとってかわられつつある．特筆すべきは，乳がんや膵がんなど，かつてはさほど多くなかったがんが次第に順位をあげていることである．これも戦後数十年以来の国民の食生活の変化を物語っているのかもしれない．胃がんの死亡者数の減少には，刺激性食物など食生活の変化はもちろんだが，世界でも先駆的なさまざまな診断および治療技術の進歩があったと思われる．胃がんをいかに早期発見するかは消化器内科医の悲願であり，いわゆる二重造影法をはじめとして，その後は胃内視鏡技術がわが国で開発され，世界に誇る技術となっている．内視鏡の製造会社としては，現在でもオリンパスなどの国内メーカーが，世界シェアの大半を占めている．消化管のがんに対しては内視鏡的手術の進歩とともに，胃がん撲滅への挑戦が続けられている．近年では放射線療法においても，がん治療技術の革新が目覚ましく，重粒子線や陽子線治療などが成果を上げている．しかるに内視鏡などの簡便な装置に比べると，放射能設備を備えた大型治療装置が必要であり，建設費用も数十億円以上かかるなど，必ずしも簡便な治療法ではない．

そこで本原稿では，内視鏡ほど簡便ではないが，重粒子線ほど複雑ではない，がんの治療法として温熱療法をまとめてみたい．とりわけ近年EU諸国で実用化された，マグフォース社による超局所選択的な温熱療法について紹介するが，さらにこの治療法を凌駕するわが国のがん治療についても知見をまとめる．現在われわれが開発を進めているのが，IHIの持つ造船技術を医薬品開発に応用したものである．いわゆる一般医薬品中から，これまで解析の対象となっていない物理的な特性を検討する手法である．創薬のツールとして，あるいは磁性を有する化合物を選んだり設計する手法であり，有機磁性体開発の新技術である．造船技術における材料開発手法の医療転用であり，今後の新薬のスクリーニングや抗がん剤など新規医薬品化合物の開発に強力な武器となると考えられる．

2．最近の抗がん治療技術の進歩

2．1　温熱療法について

がん細胞では代謝が亢進しており，いわゆる代謝に伴う活性酸素などの産生も多いことが知られている．これはがん細胞の盛んな分裂能を示していると思われる．一般に細胞は温度の上昇に伴って，酵素活性の上昇とともに代謝活性が上がることが知られている．よく知られている体温の36.5度で，われわれの体の酵素活性が最大となるので

[*1] Yoshihiro Ishikawa　横浜市立大学大学院医学研究科　循環制御医学　教授　医学博士
[*2] Haruki Eguchi　㈱IHI　技術開発本部基盤技術研究所応用理学研究部　主幹研究員　工学博士
How to treat cancer without surgery?

はなく，更に高い温度まで酵素活性が上昇する．例えば細胞内セカンドメッセンジャーを産生するアデニル酸シクラーゼは，すべての細胞に発現する基本的な細胞酵素であるが，その酵素活性は37度で最大を示すのではなく，42度まで温度依存性に上昇していく．一見すると温度が上がって酵素活性が上がることはよさそうだが，アデニル酸シクラーゼの場合でも高温化で長時間さらされると，やがて酵素活性が低下し，失活することが知られている．いったん高温にさらされて失活した酵素が，再び酵素活性を取り戻すことはない．おそらく酵素蛋白の立体構造の変化を伴って不可逆的な失活を起こしていると考えられる．

そこで，もともと代謝活性の高いがん細胞が，高温にさらされれば代謝活性はさらに上昇し，これが長く続けばがん細胞に対して殺傷効果を持つのではないかということが容易に推測できる．歴史的にも，高熱疾患にかかった患者の腫瘍が縮小したことが報告されており，がんの自然治癒症例においては発熱が何らかの原因であったという報告もある．さらに温熱によって免疫能力が高まることがさまざまな実験からも明らかとなっており，がんに対する免疫能力の亢進から，がん細胞に対する治療効果が表れるとも考えられている．このような事実から，がん組織を高熱にさらすことによって，抗がん治療を行おうという発想が生まれた．本格的な研究が始まったのは60年代以降であるが，さまざまな治療温熱装置が考案されており，治療成果を上げている．一般にはがん組織の温度が41度以上になるとがん細胞に対して殺傷効果が見られ，42.5度で理想的な殺傷効果を来すとされているが，がん細胞種にもより，温熱に対して感受性の高いがんもあれば，さほど高い感受性を示さないものもある．

2．2　全身と局所温熱について

がん細胞のみを標的にした温熱療法であるならば，がん組織の温度だけを選択的にあげればよい．周りの健常細胞も，温熱によってダメージが皆無というわけではないから，がん組織選択的な温熱療法が理想である．しかしながら，局所的な温熱療法は，物理的な手法の制限から困難である．皮膚などの体表にある病変組織であれば，局所に対して物理的なプローベを用いて温熱を付加することが容易である．しかるに深部臓器に対して臓器選択的に温熱を付加することが難しい．そこでわが国で開発されたのが，サーモトロンをはじめとする温熱治療器である．これは相対向する2枚の電極で体をはさみ，高周波エネルギーを利用してがん組織に対して加温を行い，がん殺傷効果を引き起こすものである．対抗する電極の大小の組合せや，出力の調節により，浅部から深部がんに及ぶまで温熱作用を示すことができるため，全国の施設で使用されている．しかしながら，治療効果としては必ずしも他の方法に勝っているともいえず，単独療法として行われるのではなく，他の治療法の補助療法として，あるいは緩和を目的として施行されることも多い．加温だけであるために副作用がほとんどなく，この点においては末期がんや治療困難な症例に対しても有意義と考えられる．

2．3　選択的局所温熱について

磁性鉄粒子を利用して，交流磁場印加によってそのヒステリシス特性を利用して発熱させる手法が，わが国でも盛んに研究されてきた．かつての磁性鉄粒子を直接使用した手法から，近年ではリポソームに包埋したり，表面にナノコーティングを施し，組織親和性を高めたさまざまな磁性粒子が使用されている．しかるに本邦では実用化に至るまでにさまざまな困難があり，実際の治療で汎用されるに至っていない．これに対して近年欧州で開発されたのが，磁性鉄粒子を用いた超選択的な温熱療法である．マグフォース社によって開発されたNanoActivatorという交流磁場印加装置と，NanoTermという名で販売されている酸化鉄粒子の組合せによりEUにおける認可を受けている．現在のところ適応疾患としては，神経膠芽腫のみであるが，すでにEU 27ヵ国で承認を受けており，現在EU域内では画期的な局所温熱療法として注目を集めている．治療の原理はいたって簡単で，頭蓋内の神経膠芽腫の部分に特殊コーティングを施された酸化鉄粒子を局所注入し，頭蓋を覆うように配置した交流磁場印加装置で腫瘍組織を選択的に加温するものである．発熱体として磁性鉄を使用しているために，局所が極めて高熱化し，

そのために効率的ながん細胞の殺傷効果が得られるとされる．この点において，いわゆる42.5度を目標温度としたマイルドな温熱療法に対して，高温を発生させる強力な温熱療法と呼ぶことができるだろう．

神経膠芽腫は年間の発生件数は日欧米でも数万人程度で，わが国では中年以降に発症が多く，男性に多いとされる．脳の原発性腫瘍の約1割であり，前頭葉および側頭葉に好発する．手術による根治が困難であり，一般には放射線療法と化学療法の併用が主体であり，抗がん剤としてはテモゾロミドが使用されている．遠隔転移は稀であるが，予後は極めて不良であり，5年生存率は10%に満たない．このような予後不良のがんに対して，マグフォース社の磁性粒子温熱療法がEUで認可されたのは納得がいく．しかるにその適応疾患を拡大しつつあり，現在米国のメイヨークリニックなどで，肝臓がん，前立腺がん，すい臓がんなどを対象として臨床試験が進行中である．患者数からすれば圧倒的に多いので，今後マグフォース社の超選択的温熱療法が拡大普及する可能性がある．

さらに最近のヒト肝がんに対する研究成果が報告されている．13名の肝細胞がん患者において，経動脈的に塞栓術を行った例が示されている．いわゆるがん組織の栄養動脈から，6例はリゾビストあるいはマグフォース社の鉄粒子を注入した．鉄注入量としてはいずれも数ミリグラムである．MRIによって治療前および治療後のがん細胞の状態を評価しているが，いずれもがん組織に選択的に注入され，健常組織への漏れは検出できなかったとされている[2]．本報告ではNanoActivatorによる交流磁場印加は行われていないが，本年6月のマスコミ発表で，米国のメイヨークリニックにおいて，NanoActivatorとNanoThermを用いた臨床試験が開始されたという報告が出された．本試験では肝がんのみならず，すい臓がんを対象としており，既にパイロット試験ではすい臓がんに対する有効性が示されており，これまでは難治性がんの代表であったすい臓がんに対して，画期的な治療法の開発になると考えられている．

2．3　化学療法と選択的局所温熱の併用について

上記の神経膠芽腫に対して，腫瘍局所に磁性鉄粒子を注入して，化学療法や放射線療法を併用することによって治療効果がさらに向上することが想像される．EUで行われている治療法においても，放射線療法との併用がおこなわれている．しかるに化学療法との併用は考えられていない．一見すると矛盾する概念だが，局所温熱療法では，がん組織内部に注入した酸化鉄粒子が高温化してしまい，このために抗がん剤自体が熱変性を起こしてしまう．したがって抗がん剤が局所に届いても，熱のために変性してしまうので無意味となる．そこで考えられるのが，熱によって変性しない抗がん剤である．あるいは抗がん剤自体に発熱作用，つまり磁性特性があるものである．このような薬剤化合物を選び出す，あるいは設計するのには，旧来的な医薬品評価手法では困難である．

2．4　金属材料評価技術の医学転用

IHIでは古くから船舶やジェットエンジンの設計と製造を手掛けている．材料はいずれも金属であり，場合によってはさまざまな合金が合成される．このような金属材料の物理特性は，製造の工程や条件によって変化するため，何らかの手法で最終産物である金属材料の物理特性を予測する技術が進歩した．その一つが第一原理計算であり，物理化学では標準的に使用されている手法である．この手法を有機機能材料の評価に使えないかの検討が行われた．この初期対象として選ばれたのが，細胞内酵素であるアデニル酸シクラーゼを賦活するフォルスコリンである．フォルスコリンはインド産紫蘇植物であるコレウス・フォールスコリーの抽出物であり，今から30年前にアメリカで開発された．わが国ではやせ薬として販売されているので，ご存知の方も多いと思う．アデニル酸シクラーゼには，実は9種類のサブタイプがあり，それぞれのサブタイプが組織選択的に発現する．アデニル酸シクラーゼ自身は，カテコラミン，つまり交感神経受容体刺激によって活性化されるから，アデニル酸シクラーゼの活性化は交感神経活性化と同じ作用を示す．心不全などの心機能が落ちた時には，交感神経の活性化によって心機能を亢進させることが必要であるが，いわゆるカテコラミンで刺激すると全身の交感神経受容体が活性

化されてしまい，さまざまな副作用を起こす．そこで心臓にだけ発現するアデニル酸シクラーゼサブタイプを，選択的に刺激する薬剤が開発された．この元となったのがフォルスコリンである．

200種類にもおよぶフォルスコリン誘導体に対して，薬理学的なスクリーニングを行い，アデニル酸シクラーゼのそれぞれのサブタイプを選択的に刺激する誘導体群を選び出した[3]．この検索に必要とされたのは，アデニル酸シクラーゼ酵素の蛋白質立体構造であり，いわゆる活性中心に対してフィッティングモデルを利用して，各サブタイプに選択的な誘導体をスクリーニングした．それぞれのサブタイプに選択性を示す複数の誘導体が選ばれたが，いずれも薬理的実験によって選ばれたものであり，選ばれた化合物の共通性質を推測することは，これまでの医学技術では困難であった．

そこでこれらの誘導体化合物の，化合物自体の物理特性に共通する性質を選び出すのに，第一原理計算が使われた．いずれも密度汎関数法を用いて，電子とイオンの相互作用については，全電子法によりすべての電子を考慮した．波動関数はスピン分極型の線形結合型の原子軌道で分極関数を追加した2重数値規定関数を使用した．静電ポテンシャルの分布，波動関数分布(HOMO，LUMO)，福井関数の分布を調べた結果，静電ポテンシャルの分布によって，アデニル酸シクラーゼサブタイプの選択性が予測できることが解った(図1)[4]．

この解析は二点において重要と考えた．第一は，これまでの医学的な化合物評価技術では，標的蛋白質の立体構造が必須であった．立体構造とともに，化合物がどのように標的蛋白と結合するのかのメカニズムの検討が不可欠であった．そのため蛋白構造が明らかになっていない標的に対して，この手法を用いることができなかった．さらに蛋白の結晶構造にサブタイプごとの変異があると，更に予想が困難なものとなってしまう．二点目は，蛋白構造を明らかにして，選択的な化合物を多数選び出したとしても，さらに選び出したい場合には再び蛋白質の結晶構造を用いねばならない．これは同じような方法を繰り返し使用して，新規化合物を選び出さねばならないことを意味する．もしも既に選び出された化合物の共通特性を特定因子として，そのような共通特性を持つ化合物を選ぶことができれば，創薬のスクリーニングプロセスは圧倒的に加速する．

2．5　第一原理計算と創薬

第一原理計算の医薬品スクリーニングへの応用は，上記の2点を可能とした．第一原理計算は蛋白の情報は不要で，化合物のみで解析が可能である．ある共通の薬理学的特性を持つ化合物群を網

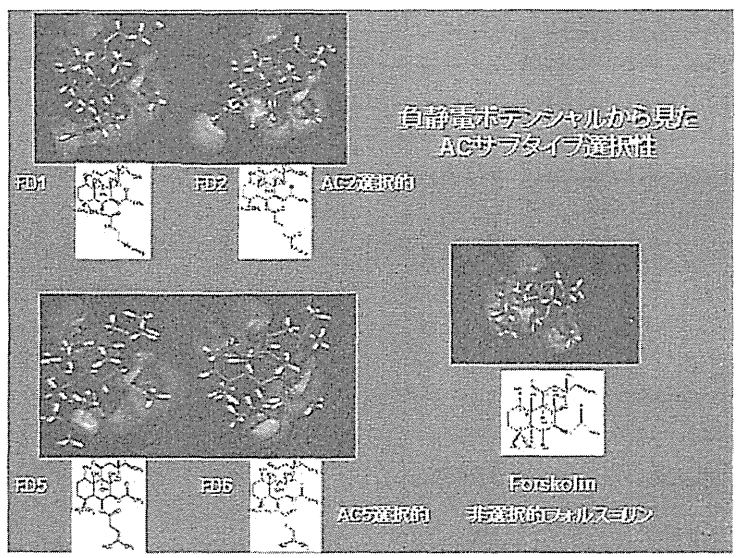

図1　フォルスコリン誘導体と負静電ポテンシャル[4]

羅的に解析し，そこから第一原理計算的に得られた共通特性を割り出す．そしてその共通特性をもつ新しい化合物に，共通の薬理学特性の存在を推測する手法である．したがって，ある数以上の共通の薬理学的性質を持つ化合物が既に存在する場合，第一原理計算を用いることによりはるかに容易に，類縁の新規化合物を選ぶことができる．一般に新薬の開発では数百あるいは数千種類の似たような化合物を用いてスクリーニングをかけることが多い．この際に本手法を導入することで相当の省力が可能となる．

第一原理計算には思わぬ副産物がついてくる．本手法は，もともとIHIにおいて金属材料の評価に使用されていた方法である．従って，医薬品に対しては要求されていないさまざまな物理学的なパラメータを解析してしまう．その一つが磁性特性である．われわれの持つフォルスコリン誘導体は有機化合物であり，医学研究者は磁性の存在を想定していない．しかるに金属材料評価の専門家にとって，磁性評価は必須項目に数えられる．われわれの磁性医薬品化合物の評価技術は，フォルスコリン誘導体の一部に磁性が同定されたことから始まった．

フォルスコリン誘導体に予測された磁性特性は，ESRによっても確認された．これによって有機化合物の一部に磁性が存在しうることが予測された．同様の方法でいわゆる一般医薬品化合物をスクリーニングした結果，複数の磁性体化合物の存在が明らかとなった．それらの化合物はSQUIDによる磁場磁化曲線解析によって，ヒステリシスループの存在が明らかとなり，いわゆる強磁性体の性質を持つことが判明した．化合物の中には，強い細胞殺傷効果を示す化合物が見つかり，細胞殺傷効果と強磁性特性を併せ持つことから，いわゆる磁性抗がん剤の可能性が示された．さまざまな検証実験から，このような化合物に対して交流磁場印加によって強い温熱効果を発揮させることも判明した．既存の抗がん剤との最大の違いは，抗がん剤自体が磁性体であるため，抗がん作用は発熱によって失われないことである．このことは，EUで実用化された磁性鉄の代わりに，磁性抗がん剤を使用することによってはるかに強い抗がん温熱療法が可能となることを意味しており，現在盛んに研究開発が行われている．

3．おわりに

わが国の高度成長期以来の蓄積で，重厚長大産業をはじめとしてさまざまな企業に膨大な技術の蓄積が行われている．しかるにそのような技術は，現在では当該産業分野では飽和的な技術となり，それ以上の新しい価値を生み出すことが少なくなっている．われわれはこれが日本の経済成長の停滞の原因の一つであると考えている．第一原理解析も，造船業や金属業においては，一般的な技術であるが，世界水準的に考えてもわが国は先端を行っている．それゆえに造船業や金属業以外に応用されることがなかった．膨大な技術と研究者の蓄積がありながら，他方面への応用が行われてこなかったことは，その必要が無かった，あるいは考えられなかったためでもあろう．第一原理計算の医薬品化合物への応用はその一例に過ぎないと考えている．おそらくわが国の化学工業技術には，まだまだ無数の技術と研究者が存在し，限られた分野にしか応用されていない技術が多数あると考える．医学応用はその一例であり，われわれのような医学部と造船業といった，通常なら考えられない異業種交流によって，新しい技術の転用が盛んとなり，日本の経済技術の成長の引き金となることを願っている．

参考文献

1) 国民衛生の動向，2011/2012，第58巻9号
2) Dudeck, O. *et al.*, *Investigative Radiology*, **41**, 527-535, 2006
3) Onda, T. *et al.*, *J. Biol. Chem.*, **276**, 47785-47793, 2001
4) Eguchi, H. and Ishikawa, Y. *Letters in Drug Design & Discovery*, 4, 434-441, 2007

ファームテクジャパン 第29巻第11号 平成25年9月1日発行（毎月1回1日発行）

PHARM TECH JAPAN

Vol.29 No.11 September 2013

9

ファームテク ジャパン